Available online at www.sciencedirect.com
SCIENCE DIRECT®
International Journal of Solids and Structures 43 (2006) 1946–1959
INTERNATIONAL JOURNAL OF SOLIDS and STRUCTURES
www.elsevier.com/locate/ijsolstr

Mixed-mode stress intensity factors for graded materials

T. Menouillard, T. Elguedj, A. Combescure *

INSA/LaMCoS, UMR/CNRS 5514, Bât. J. d'Alembert, 20 avenue Albert Einstein, 69621 Villeurbanne Cedex, France

Received 7 December 2004; received in revised form 29 April 2005
Available online 22 July 2005

Abstract

In this paper, we present a general method for the calculation of the various stress intensity factors in a material whose constitutive law is elastic, linear and varies continuously in space. The approach used to predict the stress intensity factors is an extension of the interaction integral method. For this type of material, we also develop a systematic method to derive the asymptotic displacement fields and use it to achieve better-quality results. A new analytical asymptotic field is given for two special cases of graded materials. Numerical examples focus on materials with space-dependent Young modulus.

Keywords: Energy release rate; Non-homogeneous material; Spatially variable materials; Stress intensity factor; Mixed-mode fracture; Exact crack tip asymptotic fields; X-FEM

1. Introduction

Fracture mechanics deals with the prediction of crack propagation in a material as a function of time (see Cotterell, 2002). The difficulty lies in the presence of a singularity at the crack's tip. The early works in linear elasticity were those of Griffith (1921) and Irwin (1958); they introduced the concept of energy release rate, believed to be a necessary condition for the crack to evolve (see Bui, 1978). Further, in order to take into account the direction of propagation of the crack, the concept of fracture mode must be introduced. This has already been done in the case of materials with constant mechanical properties in space (see Kim and Paulino, 2003a,b; Rao and Rahman, 2003). Here, we are focusing on the case where the mechanical properties vary continuously in space. This type of material shall be called Graded Material (see Dolbow and Gosz, 2002). The approach chosen in this paper is deliberately a macroscopic homogenised vision of the fracture of the material.

* Corresponding author. Tel.: +33 4 72 43 64 26.
E-mail addresses: thomas.menouillard@insa-lyon.fr (T. Menouillard), alain.combescure@insa-lyon.fr (A. Combescure).

0020-7683/$ - see front matter
doi:10.1016/j.ijsolstr.2005.06.021

Let Ω be a solid with elastic, linear and isotropic behavior whose constitutive relation varies continuously in space. It is subjected to static loads leading to a displacement field U and a stress field σ.

2. Stress field near the crack's tip

The problem's assumptions enable us to express the static equilibrium equation in absence of body forces as

$$\overrightarrow{\mathrm{div}}\,\sigma = \overrightarrow{0} \tag{1}$$

This is a system of first-order differential equations over the continuous domain Ω, whose solution involves basis functions (defined over the whole domain Ω) and constants which can be denoted K_{I} and K_{II} (see Bui, 1978). Using the polar coordinate system in the Cartesian framework (see Fig. 1), the stress field in the vicinity of the crack tip takes the form (at a point $M(r,\theta)$ in space)

$$[\sigma(M)] = K_{\mathrm{I}}[g_{\mathrm{I}}(M)] + K_{\mathrm{II}}[g_{\mathrm{II}}(M)] \tag{2}$$

where g_{I} and g_{II} can be viewed as the shape functions of the stress field at the crack tip (detailed expression of σ are given in Appendix A.1).

So far, no reference has been made to the material's elastic linear constitutive relation: therefore, these results are true for any spatial distribution of this relation, provided that it is continuous over the domain, Ω.

3. Displacement field near the crack's tip

3.1. Shape of the displacement field

Now, the (linear) constitutive relation can be used to derive the shape of the displacement field near the crack tip

$$\sigma = \mathbb{C} \cdot \epsilon(U) = K_{\mathrm{I}} g_{\mathrm{I}} + K_{\mathrm{II}} g_{\mathrm{II}} \tag{3}$$

Thus, the displacement field can be written as

$$U(M) = K_{\mathrm{I}} u_{\mathrm{I}}^{s}(M) + K_{\mathrm{II}} u_{\mathrm{II}}^{s}(M) \tag{4}$$

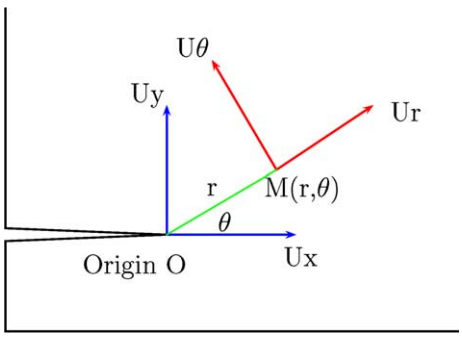

Fig. 1. Basis and coordinate system used.

The set of the solutions is the space generated by the vectors $u_{\mathrm{I}}^{s}(M)$ and $u_{\mathrm{II}}^{s}(M)$ defined by: $\mathbb{C}.\epsilon(u_i^s) = g_i$ for $i = \mathrm{I}$ and II. Let us apply this method to the following two materials:

- a material with constant mechanical properties in space: constitutive law denoted $\mathbb{C}^h$; material's asymptotic fields denoted u_i^h;
- a material with mechanical properties varying continuously in space: constitutive law denoted $\mathbb{C}^*(M)$; material's asymptotic fields denoted U_i^*.

Obviously, for $i = \mathrm{I}$ and II, one has

$$\mathbb{C}^h \cdot \epsilon(u_i^h) = \mathbb{C}^*(M) \cdot \epsilon(U_i^*) = g_i \tag{5}$$

Therefore, the asymptotic displacement fields for the material with varying characteristics in space are functions of the displacement fields for the material with constant characteristics and of the constitutive relations of the two materials considered

$$\epsilon(U_i^*) = (\mathbf{C}^*(M))^{-1} \cdot (\mathbf{C^h} \cdot \epsilon(u_i^h)) \tag{6}$$

It appears that this equation is a very general and powerful tool which allows to compute the asymptotic strain field $\epsilon(U^*)$ for any continuously varying graded material using the known asymptotic strain field of a constant mechanical property one.

Applying this result to a material with constant Poisson ratio and varying spatially Young modulus, one gets for $i = \mathrm{I}$ and II

$$\epsilon(\overrightarrow{U_i^*}) = \frac{E_0}{E(M)}\epsilon(\overrightarrow{u_i^h}) \tag{7}$$

3.2. Asymptotic displacement fields: case of a material with a varying young modulus in space and a constant poisson ratio

3.2.1. General formulation

The resolution of the differential equations (see Eq. (7)) leads to the following expression of the displacement fields (using u^h defined in Appendix A.1):

$$U_{\mathrm{I}r}^*(r,\theta) = \frac{1+\nu}{\sqrt{2\pi}}\cos\frac{\theta}{2}(k-\cos\theta)\int_0^r \frac{1}{2\sqrt{t}E(t,\theta)}\mathrm{d}t \tag{8}$$

$$U_{\mathrm{I}\theta}^*(r,\theta) = \int_0^\theta \left[\left(\frac{(1+\nu)\sqrt{2r}}{4\sqrt{\pi}E(r,\phi)}\cos\frac{\phi}{2}(k+\cos\phi-2)\right) - U_{\mathrm{I}r}(r,\phi)\right]\mathrm{d}\phi \tag{9}$$

$$U_{\mathrm{II}r}^*(r,\theta) = \frac{1+\nu}{\sqrt{2\pi}}\left[-\sin\left(\frac{\theta}{2}\right)(k+\cos\theta) + 2\sin\frac{3\theta}{2}\right]\int_0^r \frac{1}{2\sqrt{t}E(t,\theta)}\mathrm{d}t \tag{10}$$

$$\begin{aligned} U_{\mathrm{II}\theta}^*(r,\theta) = {} & \int_0^\theta \left[-\frac{(1+\nu)\sqrt{2r}}{4\sqrt{\pi}E(r,\phi)}\left(\sin\frac{\phi}{2}(k+\cos\phi-2) + 2\sin\phi\cos\frac{\phi}{2}\right)\right]\mathrm{d}\phi \\ & - \int_0^\theta U_{\mathrm{II}r}(r,\phi)\mathrm{d}\phi + f_{\mathrm{II}}(r) \end{aligned} \tag{11}$$

where Kolosov's constant k is $3-4\nu$ in plane strain or $\frac{3-\nu}{1+\nu}$ in plane stress.

Observing that Eq. (7) for asymptotic strain consists in three scalar differential equations, the function f_{II} can be determined using the third one, i.e.

$$\epsilon_{xy}(\overrightarrow{U}_i^*) = \frac{E_0}{E(x,y)}\epsilon_{xy}(\overrightarrow{u}_i^h) \tag{12}$$

This set of equations yields to the solutions of the proposed problem. In the general case, these can be obtained numerically.

3.2.2. Exact analytical case: $E(M) = E_0 e^{\alpha r}$

Two explicit exact solutions have been found for U^*. The first one is given in Appendix B.1. The second is developed in this section. The objective of this section is to develop the complete analytical expression of the asymptotic displacement fields U_{I}^* and U_{II}^* for this type of material. This material is interesting because it leads to an analytical solution:

$$U_{\mathrm{I}r}^*(r,\theta) = \frac{1+\nu}{E_0}\sqrt{\frac{r}{2\pi}}(k-\cos\theta)\cos\frac{\theta}{2}\frac{1}{\sqrt{\alpha r}}\int_0^{\sqrt{\alpha r}} \mathrm{e}^{-t^2}\mathrm{d}t \tag{13}$$

$$U_{\mathrm{I}\theta}^*(r,\theta) = \frac{1+\nu}{6E_0}\sqrt{\frac{r}{2\pi}}\left[\left((6k-9)\sin\frac{\theta}{2}+\sin\frac{3\theta}{2}\right)\mathrm{e}^{-\alpha r} + \left((6-12k)\sin\frac{\theta}{2}+2\sin\frac{3\theta}{2}\right)\frac{1}{\sqrt{\alpha r}}\int_0^{\sqrt{\alpha r}} \mathrm{e}^{-t^2}\mathrm{d}t\right] \tag{14}$$

$$U_{\mathrm{II}r}^*(r,\theta) = \frac{1+\nu}{E_0}\sqrt{\frac{r}{2\pi}}\left[-\sin\left(\frac{\theta}{2}\right)(k+\cos\theta)+2\sin\frac{3\theta}{2}\right]\frac{1}{\sqrt{\alpha r}}\int_0^{\sqrt{\alpha r}} \mathrm{e}^{-t^2}\mathrm{d}t \tag{15}$$

$$U_{\mathrm{II}\theta}^*(r,\theta) = \frac{1+\nu}{2E_0}\sqrt{\frac{r}{2\pi}}\left[\left((2k-3)\cos\frac{\theta}{2}+\cos\frac{3\theta}{2}-1-3k\right)\mathrm{e}^{-\alpha r} + \left((2-4k)\cos\frac{\theta}{2}+2\cos\frac{3\theta}{2}+3k+1-2(k+3)\alpha r\right)\frac{1}{\sqrt{\alpha r}}\int_0^{\sqrt{\alpha r}} \mathrm{e}^{-t^2}\mathrm{d}t\right] \tag{16}$$

Since these solutions are completely analytical, they can be used in calculation programs without numerical computations.

3.2.3. Partial analytical solution

Two solutions for more usual materials are given in Appendix B.1. These imply partial numerical integration.

4. Formulation of the energy release rate

Suo and Combescure (1992a,b) showed that the energy release rate can be written for space variable material as follows, using any continuous virtual displacement field Θ parallel to the crack face (Fig. 2)

$$G = \int_\Omega \mathrm{tr}(\sigma\cdot\nabla U\cdot\nabla\Theta)\cdot\mathrm{d}\Omega - \int_\Omega w\cdot\mathrm{div}(\Theta)\mathrm{d}\Omega + -\frac{1}{2}\int_\Omega \mathrm{tr}[\nabla\mathbb{C}\cdot\Theta\cdot\epsilon(U)\cdot\epsilon(U)]\mathrm{d}\Omega + \int_\Omega f\cdot U \cdot\mathrm{div}(\Theta)\mathrm{d}\Omega + \int_\Omega \nabla f\cdot\Theta\cdot U\mathrm{d}\Omega \quad \forall\Theta \tag{17}$$

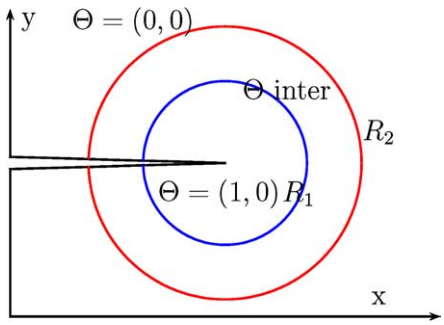

Fig. 2. Description of the field Θ near the crack's tip.

with α the thermal expansion coefficient, δT the temperature variation within the material, and with w defined by

$$w = \frac{1}{2}\mathrm{tr}[\sigma \cdot \epsilon(U)] \tag{18}$$

Remark. Eq. (17) is valid on the whole domain Ω. The choice of Θ function is arbitrary. If we chose Θ to be $(0,0)$ outside the circle R_2, G has to be computed only within the circle.

In a finite element program, such as CAST3M, the $G\Theta$ method (see Suo and Valeta, 1996; Suo and Brochard, 1991; Attigui et al., 1995) is used.

5. Mixed-mode analysis for a variable material

The method presented here relies essentially on the shape of the displacements near the crack tip. We showed the relation between the displacements and the stress intensity factors K_{I} and K_{II}. The following method enables one to calculate these stress intensity factors.

5.1. Preliminaries

First, let us introduce the following functions:

$$J: \ \mathbb{R}^4 \to \mathbb{R}(u,v) \mapsto J(u,v) = a(u,v)$$

where

- $a(\cdot,\cdot)$ is a symmetric bilinear form defined as

$$a(u,v) = \int_\Omega \mathrm{tr}[\mathbb{C} \cdot \epsilon(u) \cdot \nabla v \cdot \nabla \Theta + \mathbb{C} \cdot \epsilon(v) \cdot \nabla u \cdot \nabla \Theta - (\mathrm{div}(\Theta) \cdot \mathbb{C} + \nabla \mathbb{C} \cdot \Theta) \cdot \epsilon(u) \cdot \epsilon(v)]\mathrm{d}\Omega$$

These functions have the following property: if U is the actual displacement field, then

$$J(U,U) = 2 \cdot G = a(U,U) \tag{19}$$

Let u_{I}^s and u_{II}^s be two fields characterizing Mode I and Mode II in displacement. By choosing $U = K_{\mathrm{I}} u_{\mathrm{I}}^s + K_{\mathrm{II}} u_{\mathrm{II}}^s$, one gets

$$G = \frac{1}{2} a(u_{\mathrm{I}}^s, u_{\mathrm{I}}^s) K_{\mathrm{I}}^2 + \frac{1}{2} a(u_{\mathrm{II}}^s, u_{\mathrm{II}}^s) K_{\mathrm{II}}^2 + a(u_{\mathrm{I}}^s, u_{\mathrm{II}}^s) K_{\mathrm{I}} K_{\mathrm{II}}$$

5.2. The method

In order to determine the two scalars (K_{I} and K_{II}), one must write two scalar equations involving the two quantities; let us apply the bilinear form $a(\cdot,\cdot)$ to two pairs of displacement fields

$$\begin{cases} a(U,u_{\mathrm{I}}^s) = K_{\mathrm{I}}a(u_{\mathrm{I}}^s,u_{\mathrm{I}}^s) + K_{\mathrm{II}}a(u_{\mathrm{II}}^s,u_{\mathrm{I}}^s) \\ a(U,u_{\mathrm{II}}^s) = K_{\mathrm{I}}a(u_{\mathrm{I}}^s,u_{\mathrm{II}}^s) + K_{\mathrm{II}}a(u_{\mathrm{II}}^s,u_{\mathrm{II}}^s) \end{cases} \tag{20}$$

The solutions are

$$K_{\mathrm{I}} = \frac{a(u_{\mathrm{II}}^s,u_{\mathrm{II}}^s)\cdot a(U,u_{\mathrm{I}}^s) - a(u_{\mathrm{I}}^s,u_{\mathrm{II}}^s)\cdot a(U,u_{\mathrm{II}}^s)}{a(u_{\mathrm{I}}^s,u_{\mathrm{I}}^s)\cdot a(u_{\mathrm{II}}^s,u_{\mathrm{II}}^s) - a(u_{\mathrm{I}}^s,u_{\mathrm{II}}^s)^2} \tag{21}$$

$$K_{\mathrm{II}} = \frac{a(u_{\mathrm{I}}^s,u_{\mathrm{I}}^s)\cdot a(U,u_{\mathrm{II}}^s) - a(u_{\mathrm{I}}^s,u_{\mathrm{II}}^s)\cdot a(U,u_{\mathrm{I}}^s)}{a(u_{\mathrm{I}}^s,u_{\mathrm{I}}^s)\cdot a(u_{\mathrm{II}}^s,u_{\mathrm{II}}^s) - a(u_{\mathrm{I}}^s,u_{\mathrm{II}}^s)^2} \tag{22}$$

Remark 1. If the material is constant, then

$$a(u_{\mathrm{I}}^h,u_{\mathrm{I}}^h) = \frac{2(1-\nu^2)}{E_0}, \quad a(u_{\mathrm{II}}^h,u_{\mathrm{II}}^h) = \frac{2(1-\nu^2)}{E_0}, \quad a(u_{\mathrm{I}}^h,u_{\mathrm{II}}^h) = 0 \tag{23}$$

Thus, the stress intensity factors can be written

$$K_{\mathrm{I}} = \frac{E_0 a(U,u_{\mathrm{I}}^h)}{2(1-\nu^2)}, \quad K_{\mathrm{II}} = \frac{E_0 a(U,u_{\mathrm{II}}^h)}{2(1-\nu^2)} \tag{24}$$

This particular case agrees with published results (Visse, 1995).

Remark 2. Eqs. (21) and (22) are new because of the presence of term $a(u_{\mathrm{I}}^s,u_{\mathrm{II}}^s)$ which is compulsory when the material is spatially variable and vanishes when material is constant.

5.3. Use of the asymptotic fields of the constant material for a variable material

The space variation of the material raises the question of the choice of the field u_i^s in the formulation of the stress intensity factors. One can use either u_i^h or U_i^*. However, one may anticipate that the quality of the results will depend on the asymptotic fields chosen for the uncoupling. Near the crack tip, the fields u_i^h give a good approximation because the material's characteristics are continuous. However, as the distance to the crack tip increases, these fields become less good than the fields U_i^*, which take into account the variation of the material's characteristics. The numerical examples will illustrate these points.

In this section, we chose to use the asymptotic h fields. Table 1 shows the analytical results of the calculations of $a(u_i^h,u_j^h)$ for different type of spatially variable Young modulus. In particular, it shows the evolution of $a(u_i^h,u_j^h)$ as a function of the radius R of the crown Θ. One can see that the error of the prediction of K_{I} and K_{II} is proportional to the product of the proportionally constant ψ, β, γ by the radius R in case of linear dependency and to R^2 in case of quadratic dependency. It is clear in this case that the use of u^h displacement fields to uncouple the K_i implies a very fine mesh close to the crack tip to have a good accuracy.

Remark. One should note that for any continuous material (denoting $E(0,0) = E_0$)

$$\lim_{R\to 0} a(u_{\mathrm{I}}^h,u_{\mathrm{I}}^h) = \frac{2(1-\nu^2)}{E_0}, \quad \lim_{R\to 0} a(u_{\mathrm{II}}^h,u_{\mathrm{II}}^h) = \frac{2(1-\nu^2)}{E_0}, \quad \lim_{R\to 0} a(u_{\mathrm{I}}^h,u_{\mathrm{II}}^h) = 0 \tag{25}$$

Table 1
Table showing the error in the coefficients $a(u_i^h, u_j^h)$ as a function of the radius R of the crown Θ for several type of spatial variations of the Young modulus

Error in $a(u_i^h, u_j^h)$			
$E(x,y)$	$a(u_{\mathrm{I}}^h, u_{\mathrm{I}}^h) - \frac{2(1-\nu^2)}{E_0}$	$a(u_{\mathrm{II}}^h, u_{\mathrm{II}}^h) - \frac{2(1-\nu^2)}{E_0}$	$a(u_{\mathrm{I}}^h, u_{\mathrm{II}}^h)$
E_0	0	0	0
$E_0 + \psi x$	$-2.99\frac{\psi R}{E_0^2}$	$-1.21\frac{\psi R}{E_0^2}$	0
$E_0 + \beta y$	0	0	$0.24\frac{\beta R}{E_0^2}$
$E_0 + \gamma x\ y$	0	0	$0.58\frac{\gamma R^2}{E_0^2}$

6. Numerical examples

First, the validation of the formulation of the stress intensity factors will enable us to focus on the choice of u_i^s and more particularly on the influence of the radius of the field Θ on the results. Since the fields U_i^* become closer to the true solution than the fields u_i^h as the distance to the crack tip increases, they lead to results that are less dependent on the size of the field Θ. We will observe this difference in a finite element program (CAST3M Suo and Combescure, 1992a) and in a program using the eXtended Finite Element Method (X-FEM, Moes et al., 1999; Moes et al., 2002). Finally, the X-FEM will enable us to consider the case of an inclined crack.

6.1. Validation of the formulation

In order to validate the method described in the previous sections, the paper Kim and Paulino, 2003a will be used as the reference. The characteristics of the test are presented in Fig. 3 (displacement loading $\overline{\epsilon} = 1$). The programming of the bilinear form $a(\cdot,\cdot)$ is the core of this validation. The normalised stress intensity factors ($\widetilde{K}_{\mathrm{I}}$) are defined as follows:

$$\widetilde{K}_{\mathrm{I}} = \frac{K_{\mathrm{I}}}{\overline{\epsilon}\overline{E}(-0.4)\sqrt{\pi a}} \tag{26}$$

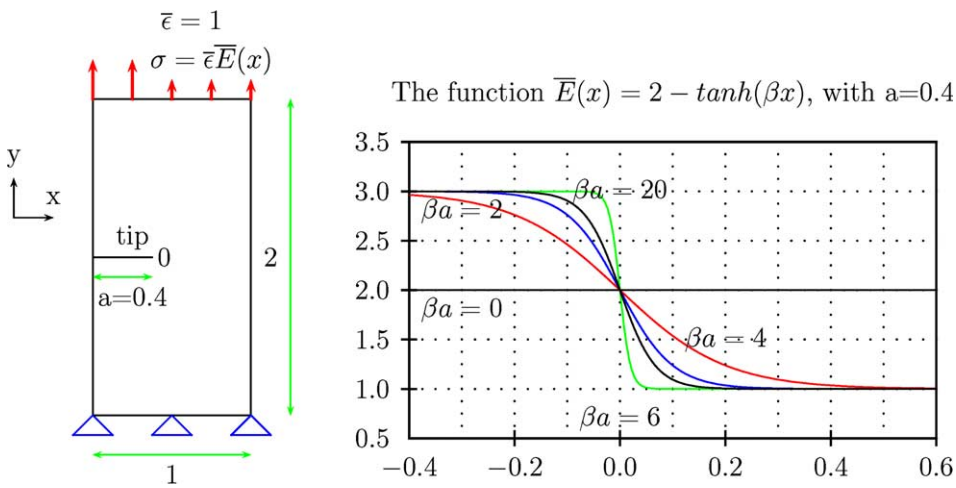

Fig. 3. Numerical validation: geometry, loading, Young modulus.

Let us recall that the expression of the stress intensity factor for Mode I is

$$K_{\mathrm{I}} = \frac{a(u^s_{\mathrm{II}}, u^s_{\mathrm{II}}) \cdot a(U, u^s_{\mathrm{I}}) - a(u^s_{\mathrm{I}}, u^s_{\mathrm{II}}) \cdot a(U, u^s_{\mathrm{II}})}{a(u^s_{\mathrm{I}}, u^s_{\mathrm{I}}) \cdot a(u^s_{\mathrm{II}}, u^s_{\mathrm{II}}) - a(u^s_{\mathrm{I}}, u^s_{\mathrm{II}})^2} \tag{27}$$

How should one choose the asymptotic fields to be used in the calculation of K_{I}? Let us choose to use the asymptotic fields of a material whose mechanical characteristics are constant (values taken at the crack tip). Thus, these are approximate fields. We are going to focus on the influence of the radius of the field Θ on the results.

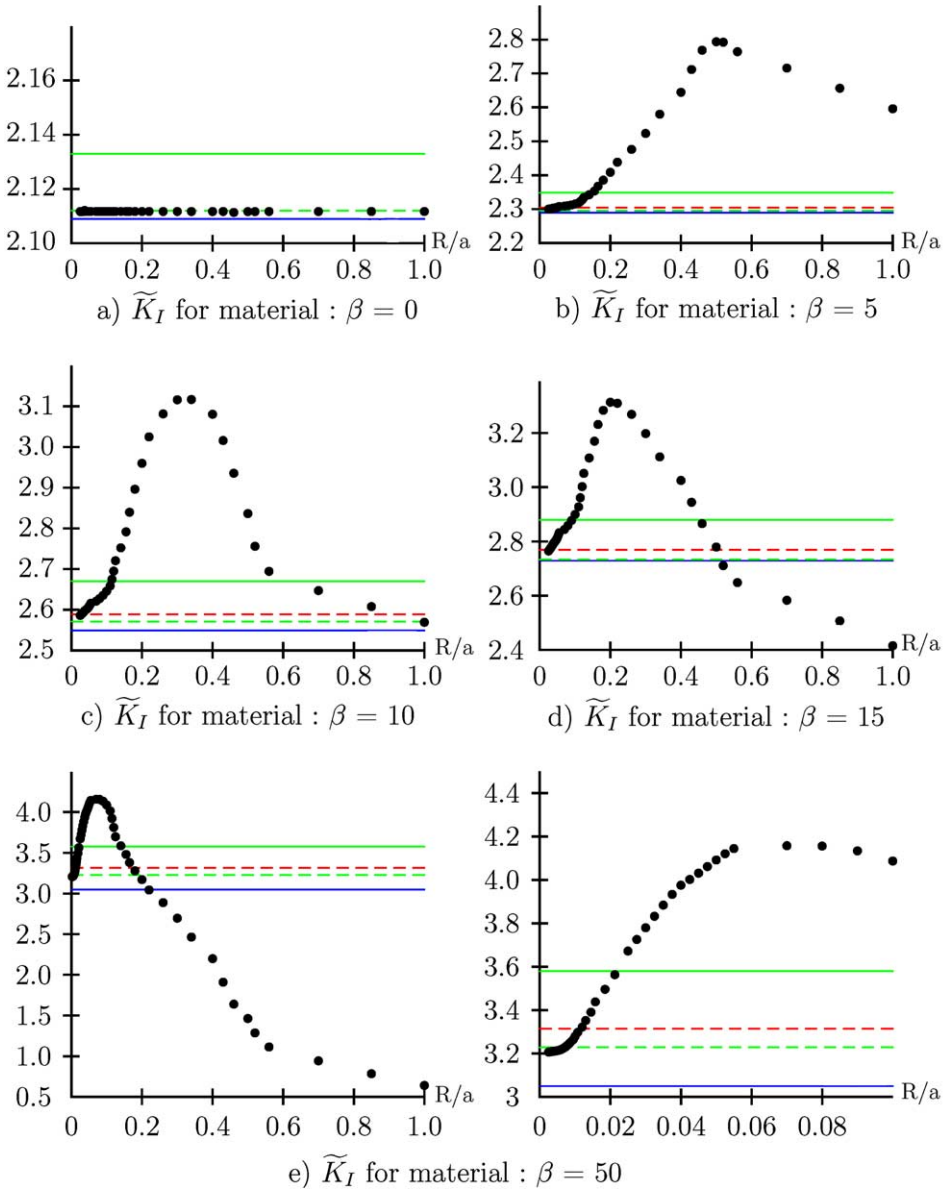

Fig. 4. Results of the numerical validation.

Table 2
Table of the test results compared to the results of Kim and Paulino (2003a)

β	βa	Direct	Method I	Method II	Eischen	This method
0	0	2.109	2.133	2.133	2.112	2.1118
5	2	2.289	2.304	2.348	2.295	2.300
10	4	2.549	2.589	2.670	2.571	2.586
15	6	2.729	2.769	2.879	2.733	2.765
50	20	3.050	3.314	3.579	3.228	3.207

Table 3
Table of the maximum crown radius as a function of the maximum error allowed on K_I

β	βa	R/a max for the following allowable errors		
		Error on K_I: 5% (%)	Error on K_I: 10% (%)	Error on K_I: 20% (%)
5	2	19	33	39
10	4	13	21	32
15	6	8	13	21
50	20	1.5	2	3

As expected in previous section, the influence of the radius of the crown can be observed, and the greater the variation of the modulus, the smaller a radius it takes to achieve an acceptable result. This can be explained by the variability of the Young modulus. Fig. 4 shows the calculated $\widetilde{K}_I$ (black dots) as functions of the crown of virtual field Θ used for various Young moduli. In addition, the horizontal lines represent the results of the works of Kim and Paulino (2003a). These authors proposed various methods which are summarized in Table 2 and compared to the results of Fig. 4. The continuous black line corresponds to the Direct Method, the continuous grey line to Method II, the dotted black line to Method I and the dotted grey line to the Eischen Method.

Convergence of the results occurred as soon as the Young modulus converged towards E_0 (value at the crack tip). The maximum acceptable radius of a crown as a function of β is shown in Table 3. The conclusion is that when the variation of Young modulus is large near the crack tip, a very fine mesh is needed to get a good K_I value. R/a has to be around 1%.

6.2. Choice of the asymptotic solutions in the calculation of the stress intensity factors

The advantage of the method presented resides in the available asymptotic solutions to choose from. By enriching the information in these solutions one can use larger Θ crowns (and, therefore, larger elements in these crowns). In the end, enriching the asymptotic solutions reduces the number of elements near the crack tip.

For a given error on the stress intensity factors, richer solutions enable one to use a larger field.

The enrichment of the asymptotic displacement fields yields greater independence with respect to the radius of the circular field.

Fig. 5 describes the mechanical problem. The quality of the prediction of K_I and K_{II} with a standard finite element solution and with the two u^h and U^* fields are compared for Finite Element CAST3M in Fig. 6 and X-FEM in Fig. 7.

Fig. 8 shows the relative error in the calculated stress intensity factor K_I as a function of the radius of the field and of the asymptotic solutions chosen for the two calculation cases (CAST3M and X-FEM). This is a very interesting graph as it shows two things: first, the computational effectiveness of the X-FEM compared to the finite element method (CAST3M). The results with the X-FEM are virtually

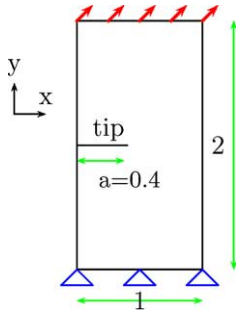

Fig. 5. Geometry of the mixed-mode test case (Young modulus is: $E(M) = E_0 e^{\alpha r}$).

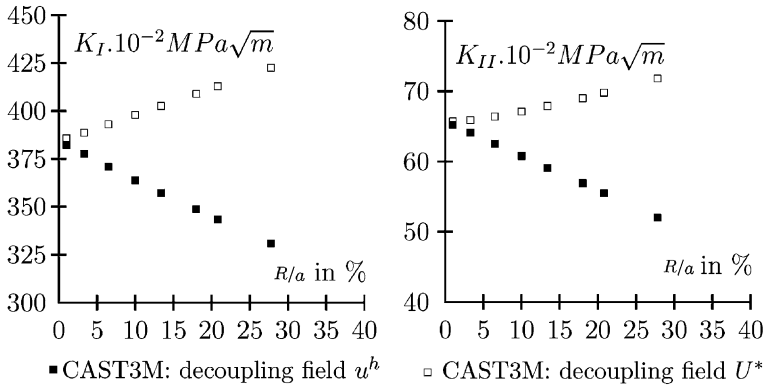

Fig. 6. Influence of the radius of the Θ crown on the calculation of K_I and K_{II} with CAST3M.

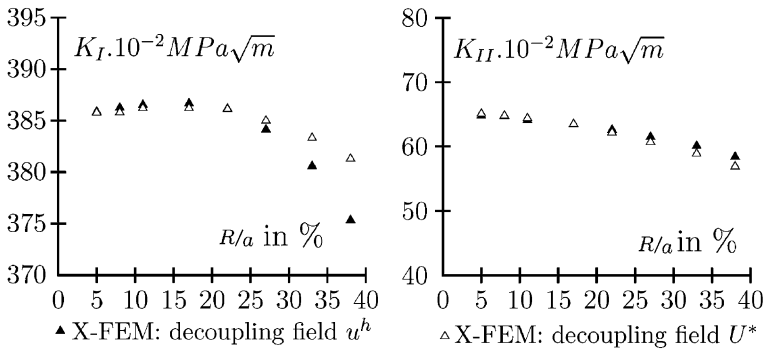

Fig. 7. Influence of the radius of the Θ crown on the calculation of K_I and K_{II} with X-FEM.

independent of the crown (see Figs. (21) and (22)). This is due to the fact that the extended enriched functions contained all the ingredients and thus the minimisation done with the linear system solution leads to automatic adjustment of the coefficients in an energetic norm. Second, using the asymptotic solutions of

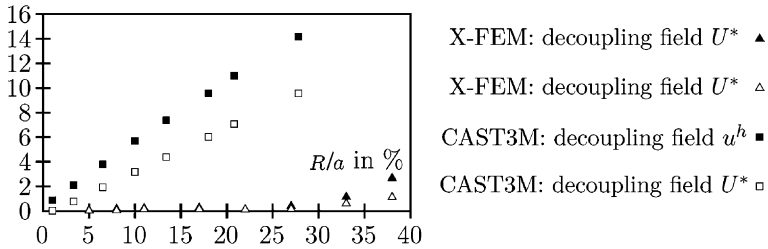

Fig. 8. Relative error (in %) in K_I as a function of the radius of the Θ field's crown.

the variable material for decoupling leads to smaller errors than using asymptotic solutions of the constant material.

6.3. X-FEM: inclined crack in a graded material

A diagram of the test is shown in Fig. 9. Since the material does not lend itself to the analytical determination of the asymptotic solutions, decoupling was achieved using the displacement fields of the constant material (value at the crack tip for the actual material). The results for crack angles 0°, 30°, 40° and 60° in the material ($E(M) = 2e^{3x}$) are shown in Figs. 10 and 11.

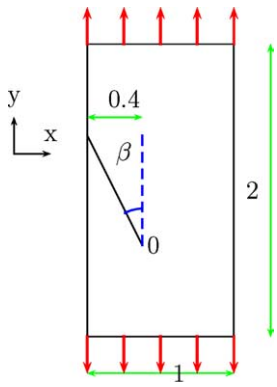

Fig. 9. Inclined crack: geometry and loading (Young modulus is: $E(M) = E_0 e^{\alpha x}$).

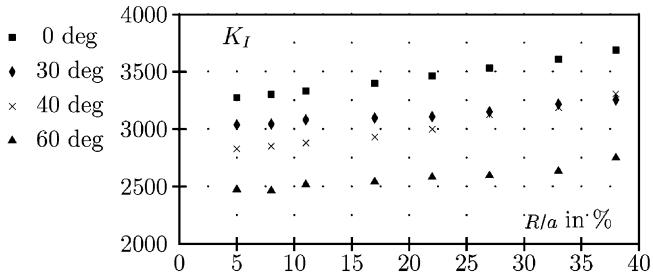

Fig. 10. Influence of the radius of the Θ field's crown on the calculation of K_I for an FGM in mixed mode, for various crack angles β.

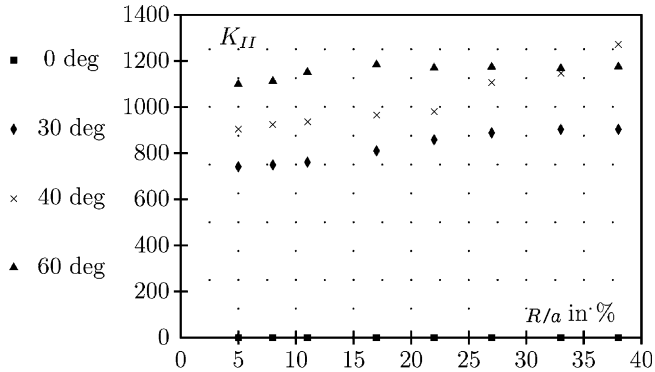

Fig. 11. Influence of the radius of the Θ field's crown on the calculation of K_{II} for a FGM in mixed mode, for various crack angles β.

Figs. 10 and 11 indicate a certain stability of the results with respect to the Θ field's crown: the error in the stress intensity factors is 20% at the most for a radius of the crown equal to 40% of the crack's length (which is an extremely large crown). A reasonable crown size is no more than 20% of the crack's length, which corresponds to an error in the stress intensity factors of 10%.

7. Conclusion and future works

The uncoupling of the fracture modes involves a virtual crown (e.g. field Θ). From a computational standpoint, it is preferable for the results not to depend on the radius of this crown. This is indeed the case for a constant material. Conversely, for a variable material, the material's characteristics vary within the crown and, therefore, the use of the displacement fields of the constant material induces a sensitivity to the radius of the crown. We achieved better stability by using the variable constitutive relation along with the asymptotic fields of the variable material.

However, in most cases, there is no exact asymptotic solution for the material $E(X)$. The X-FEM tool produced much better results than standard finite element approach because of the presence in the extended functions of all basic function of the fields ie $\sqrt{r}\{\cos(\theta/2), \sin(\theta/2), \cos(3\theta/2), \sin(3\theta/2)\}$ and the technique is hence highly recommended even if there is no exact asymptotic solution to efficiently decouple K_{I} and K_{II}.

Appendix A

A.1. Asymptotic stress field: case of a material with constant characteristics

$$\sigma_{xx}(r,\theta) = \frac{1}{\sqrt{2\pi r}}\left[K_{\mathrm{I}}\cos\frac{\theta}{2}\left(1-\sin\frac{\theta}{2}\sin\frac{3\theta}{2}\right) - K_{\mathrm{II}}\sin\frac{\theta}{2}\left(2+\cos\frac{\theta}{2}\cos\frac{3\theta}{2}\right)\right]$$

$$\sigma_{yy}(r,\theta) = \frac{1}{\sqrt{2\pi r}}\left[K_{\mathrm{I}}\cos\frac{\theta}{2}\left(1+\sin\frac{\theta}{2}\sin\frac{3\theta}{2}\right) - K_{\mathrm{II}}\sin\frac{\theta}{2}\cos\frac{\theta}{2}\cos\frac{3\theta}{2}\right]$$

$$\sigma_{xy}(r,\theta) = \frac{1}{\sqrt{2\pi r}}\left[K_{\mathrm{I}}\sin\frac{\theta}{2}\cos\frac{\theta}{2}\cos\frac{3\theta}{2} - K_{\mathrm{II}}\cos\frac{\theta}{2}\left(1-\sin\frac{\theta}{2}\sin\frac{3\theta}{2}\right)\right]$$

A.2. Asymptotic displacement fields: case of a material with constant characteristics

$$u^h_{\mathrm{I}r}(r,\theta) = \frac{1+\nu}{E_0}\sqrt{\frac{r}{2\pi}}\cos\left(\frac{\theta}{2}\right)(k-\cos\theta)$$

$$u^h_{\mathrm{I}\theta}(r,\theta) = -\frac{1+\nu}{E_0}\sqrt{\frac{r}{2\pi}}\sin\left(\frac{\theta}{2}\right)(k-\cos\theta)$$

$$u^h_{\mathrm{II}r}(r,\theta) = \frac{1+\nu}{E_0}\sqrt{\frac{r}{2\pi}}\left[-\sin\left(\frac{\theta}{2}\right)(k+\cos\theta)+2\sin\frac{3\theta}{2}\right]$$

$$u^h_{\mathrm{II}\theta}(r,\theta) = -\frac{1+\nu}{E_0}\sqrt{\frac{r}{2\pi}}\left[\cos\left(\frac{\theta}{2}\right)(k+\cos\theta)-2\cos\frac{3\theta}{2}\right]$$

Appendix B

B.1. Young's modulus: $E(r,\theta) = E_0 + E_{,r}r$

$$U^*_{\mathrm{I}r}(r,\theta) = \frac{1+\nu}{E_0}\sqrt{\frac{r}{2\pi}}\cos\frac{\theta}{2}(k-\cos\theta)\sqrt{\frac{E_0}{E_{,r}r}}\arctan\sqrt{\frac{E_{,r}r}{E_0}}$$

$$U^*_{\mathrm{I}\theta}(r,\theta) = \frac{1+\nu}{6}\sqrt{\frac{r}{2\pi}}\left[\frac{\sin\frac{3\theta}{2}+(6k+9)\sin\frac{\theta}{2}}{E_0+E_{,r}r}+\frac{2\sin\frac{3\theta}{2}-(12k-6)\sin\frac{\theta}{2}}{E_0}\sqrt{\frac{E_0}{E_{,r}r}}\arctan\sqrt{\frac{E_{,r}r}{E_0}}\right]$$

$$U^*_{\mathrm{II}r}(r,\theta) = \frac{1+\nu}{E_0}\sqrt{\frac{r}{2\pi}}\left[-\sin\frac{\theta}{2}(k+\cos\theta)+2\sin\frac{3\theta}{2}\right]\sqrt{\frac{E_0}{E_{,r}r}}\arctan\sqrt{\frac{E_{,r}r}{E_0}}$$

$$U^*_{\mathrm{II}\theta}(r,\theta) = \frac{1+\nu}{2}\sqrt{\frac{r}{2\pi}}\left[\frac{\cos\frac{3\theta}{2}+(2k-3)\cos\frac{\theta}{2}+4-4k+\frac{2E_{,r}r}{E_0}(1-k)}{E_0+E_{,r}r}\right.$$
$$\left.+\frac{2\cos\frac{3\theta}{2}+(2-4k)\cos\frac{\theta}{2}-4(1-k)}{E_0}\sqrt{\frac{E_0}{E_{,r}r}}\arctan\sqrt{\frac{E_{,r}r}{E_0}}\right]+f_{\mathrm{II}}(r)$$

B.2. Young's modulus: $E(x,y) = E_0 + E_{,x}x$

Two analytical integrations for $U_{\mathrm{I}r}$ and $U_{\mathrm{II}r}$ (from Eqs. (8) and (10))

$$U^*_{\mathrm{I}r}(r,\theta) = \frac{1+\nu}{E_0}\sqrt{\frac{r}{2\pi}}\cos\frac{\theta}{2}(k-\cos\theta)\sqrt{\frac{E_0}{E_{,x}r\cos\theta}}\arctan\sqrt{\frac{E_{,x}r\cos\theta}{E_0}}$$

$$U^*_{\mathrm{II}r}(r,\theta) = \frac{1+\nu}{E_0}\sqrt{\frac{r}{2\pi}}\left[-\sin\frac{\theta}{2}(k+\cos\theta)+2\sin\frac{3\theta}{2}\right]\sqrt{\frac{E_0}{E_{,x}r\cos\theta}}\arctan\sqrt{\frac{E_{,x}r\cos\theta}{E_0}}$$

And two numerical integrations for $U_{\mathrm{I}\theta}$ and $U_{\mathrm{II}\theta}$ (see Eqs. (9) and (11)).

B.3. Functionally graded materials: $E(x, y) = E_0 e^{\beta x}$

Two analytical integrations for $U_{\mathrm{I}r}$ and $U_{\mathrm{II}r}$ (from Eqs. (8) and (10))

$$U^*_{\mathrm{I}r}(r,\theta) = \frac{1+\nu}{E_0}\sqrt{\frac{r}{2\pi}}(k-\cos\theta)\cos\frac{\theta}{2}\frac{1}{\sqrt{\beta r\cos\theta}}\int_0^{\sqrt{\beta r\cos\theta}} \mathrm{e}^{-t^2}\,\mathrm{d}t$$

$$U^*_{\mathrm{II}r}(r,\theta) = \frac{1+\nu}{E_0}\sqrt{\frac{r}{2\pi}}\left[-\sin\left(\frac{\theta}{2}\right)(k+\cos\theta)+2\sin\frac{3\theta}{2}\right]\frac{1}{\sqrt{\beta r\cos\theta}}\int_0^{\sqrt{\beta r\cos\theta}} \mathrm{e}^{-t^2}\,\mathrm{d}t$$

And two numerical integrations for $U_{\mathrm{I}\theta}$ and $U_{\mathrm{II}\theta}$ (see Eqs. (9) and (11)).

References

Attigui, M.P., et Petit, M., et Valeta, C., 1995. Identification des paramètres de fissuration par la méthode g theta. Rapport DMT 95-675, CEA Saclay.

Bui, H.D., 1978. Mécanique de la rupture fragile. Masson.

Cotterell, B., 2002. The past, present, and future of fracture mechanics. Engineering Fracture Mechanics 69, 533–563.

Dolbow, J., Gosz, M., 2002. On the computation of mixed-mode stress intensity factors in functionally graded materials. International Journal of Solids and Structures 39, 2557–2574.

Griffith, A.A., 1921. The phenomena of rupture and flow in solids. Philosophical Transactional of Royal Society of London A 221, 163–198.

Irwin, G.R., 1958. Fracture, Handbuch der Physik, vol. IV. Springer-Verlag, Berlin, pp. 551–590.

Kim, J.-H., Paulino, G.H., 2003a. An accurate scheme for mixed-mode fracture analysis of functionally graded materials using the interaction integral and micromechanics models. International Journal for Numerical Methods in Engineering 58, 1457–1497.

Kim, J.-H., Paulino, G.H., 2003b. Mixed mode J-integral formulation and implementation using graded elements for fracture analysis of nonhomogeneous orthotropic materials. Mechanics of Materials 35, 107–128.

Moes, N., Dolbow, J., Belytschko, T., 1999. A finite element method for crack growth without remeshing. International Journal for Numerical Methods in Engineering 46, 131–150.

Moes, N., Gravouil, A., Belytschko, T., 2002. Non-planar 3d crack growth by the extended finite and level sets. International Journal for Numerical Methods in Engineering 53, 2549–2568.

Rao, B.N., Rahman, S., 2003. Mesh-free analysis of cracks in isotropic functionally graded materials. Engineering Fracture Mechanics 70, 1–27.

Suo, X.Z., Combescure, A., 1992a. On the application of $g(\theta)$ method and its comparison with de Lorenzi's approach. Nuclear Engineering and Design 135, 207–224.

Suo, X.Z., Combescure, A., 1992b. Energy release rate and integral for any non homogeneous material. The American Society of Mechanical Engineers 233, 173–179.

Suo, X.Z., Valeta, M.P., 1996. Quelques remarques sur l'utilisation de la méthode g(θ) pour les éléments de coques implantés dans castem 2000. Rapport DMT 96-305, CEA Saclay.

Suo, X.Z., Brochard, J., 1991. Introduction dans castem2000 de la méthode g(θ) pour les éléments coques minces. Rapport DMT 91-279, CEA Saclay.

Visse, E., 1995. Découplage des modes de rupture par une méthode énergetique. Rapport edf, EDF Direction des Etudes et Recherches.